Resistance and speed penalty of a naval ship with hull roughness

Woo-seok Choi[a], Gyeong-seo Min[a], Sang-seok Han[a], Hae-chan Yun[a], Momchil Terziev[b], Saishuai Dai[b], Daejeong Kim[c], Soonseok Song[a]*

[a]Department of Naval Architecture & Ocean Engineering, Inha University, South Korea

[b]Department of Naval Architecture, Ocean and Marine Engineering, University of Strathclyde, Glasgow, UK

[c]Division of Navigation Convergence Studies, Korea Maritime & Ocean University, South Korea

*Corresponding author email: s.song@inha.ac.kr

Abstract

Hull roughness, attributed to factors such as corrosion, the degradation of marine coatings, and, notably, biofouling colonisation, leads to increased fuel consumption, thus entailing significant environmental and economic penalties. While this issue on commercial ships is well documented in recent studies, the specific impact on the speed of warships has received limited attention. To fill this gap, this research quantifies the resistance and power penalties, as well as the speed reduction under various fouling scenarios, and explores the resultant changes in flow characteristics around the hull. For this purpose, full-scale simulations of a naval ship, specifically the DTMB 5415, utilise the unsteady Reynolds Averaged Navier-Stokes (URANS) method. A modified wall function model was incorporated into the numerical model to accurately simulate the effects of surface roughness.

Keywords: Biofouling, Computational Fluid Dynamics (CFD), DTMB 5415, Ship resistance, Speed penalty

1 Introduction

International Maritime Organization (IMO) has approved a revised initial strategy to raise the 2050 carbon emissions reduction target in the shipping industry from 50% to 100% compared to 2008 (IMO, 2023). As IMO's Greenhouse Gas Strategy is adjusted upward, it is important to optimise the energy efficiency of ships.

There are several methods to enhance the energy efficiency of ships, including hull shape optimisation (e.g. Choi, 2015; Hakim et al., 2023; Seok et al., 2019; Tran et al., 2023; Trimulyono et al., 2023), route optimisation (e.g. Taskar and Anderson, 2020; Zis et al., 2020), keeping the hull surface free from hindrances (e.g. Comas et al., 2021; Degiuli et al., 2023; Demirel et al., 2019; Farkas et al., 2021; Schultz, 2007) and the use of environmentally friendly engine types and fuel (e.g. Arifin et al., 2022; Brynolf et al., 2016; Felayati et al., 2021a, 2021b; Tuswan et al., 2023), etc. Together, these measures can collectively make a significant contribution to energy saving and environmental impact reduction in the shipping industry.

One of the effective strategies to prevent the decrease in ship efficiency is to maintain a smooth hull surface. The hull roughness of a ship increases over time due to various factors, such as corrosion and biofouling.

Increased hull roughness has effects such as speed penalty at constant power and additional fuel consumption to maintain a constant speed (Townsin, 2003). Both have negative economic and environmental impacts through increased fuel consumption and atmospheric emissions, including greenhouse gas (GHG). IMO emphasises the need for research on biofouling and operates research initiatives such as the Glo Fouling Partnership, and International Towing Tank Conference (ITTC) also created a new section on biofouling in the most recent, 29th Resistance & Propulsion Committee report (ITTC, 2021). According to a report published by the Marine Environment Protection Committee (MEPC), one of the committees within IMO, there is interest in biofouling, including reducing greenhouse gas emissions through biofouling management (IMO, 2021). Accurately predicting the increase in resistance caused by biofouling is crucial to achieving this goal.

One approach to predicting the impact of roughness on ship resistance is Granville's similarity law scaling (1958, 1978), which has garnered widespread acceptance among researchers over the years (Schultz, 2002, 2004; Schultz and Flack, 2007; Monty et al., 2016; Pullin et al., 2017; Utama et al., 2021; Demirel et al., 2017b, 2019; Song et al., 2023). This method efficiently predicts the impact of roughness on the skin friction of a flat plate by utilising the surface's roughness function—a premise widely regarded as logical and corroborated by its alignment with other advanced methods. This method is quick, robust, and in good agreement with other high-fidelity methods.

Schultz et al. (2011) studied the increase in resistance and required shaft power of battleships and found that this could result in additional expenditures of $54 million per year. This sheds light on the significant economic losses incurred by warships. However, the above study only confirmed the increase in resistance and required shaft power due to increased roughness. An increase in the roughness of a battleship not only increases fuel consumption due to increased resistance but also has a significant impact on survivability due to a decrease in ship speed. Monty et al. (2016) predicted the drag on a fouled full-scale ship using experimental results. To achieve this, they employed a modified method for predicting the total drag of a spatially developing turbulent boundary layer (TBL).

However, its assumption of a flat plate limits its applicability, as it does not account for the three-dimensional effects crucial for understanding the full spectrum of roughness impacts on the ship resistance components that are inherently tied to the vessel's three-dimensional hull shape. Thus this method only concerns the frictional resistance, while recent studies claim the roughness effect on other resistance components (Demirel et al., 2017a, Song et al., 2019a). The limitations inherent in Granville's flat plate method have been effectively addressed using Computational Fluid Dynamics (CFD). Offering a significant advantage, CFD transcends these restrictions by enabling simulations that, when performed at full scale, are free from scale effects. Furthermore, CFD simulations are capable of calculating local frictional velocities for each discretised cell. This allows for the incorporation of varying roughness Reynolds numbers and their respective roughness functions directly into the computations, providing a more nuanced and accurate analysis of roughness effects (Demirel et al., 2017a). It has the disadvantage of being more time-consuming compared to the similarity law scaling, whereas this drawback has been compensated by the recent advances in the computing power and CFD techniques.

With the predictability of roughness effects via CFD, numerous researchers have employed this technology to explore the impact of biofouling on various aspects of ship performance. This includes studies on ship resistance (e.g., Demirel et al., 2014; Demirel et al., 2017a; Farkas et al., 2019a; Song et al., 2019b) and propeller performance (e.g., Owen et al., 2018; Song et al., 2019a; 2020b), as well as investigations into ship self-propulsion characteristics (e.g., Song et al., 2020a; Farkas et al., 2020).

These studies offer significant insights into employing CFD for examining the effects of roughness. However, the bulk of research on roughness effects predominantly concentrates on merchant vessels, such as the KCS and KVLCC2. In comparison, investigations into the impact on naval ships have been relatively limited.

To the best of the authors' knowledge, there exists no CFD study investigating the roughness effect on naval ships' hydrodynamic performance. Especially from the perspective of a surface combatant, the speed penalty can be of greater importance than the increase in fuel consumption and greenhouse gas emissions. Thus, this study aims to address this gap by conducting CFD simulations on a benchmark ship hull of a surface combatant: the David Taylor Model Basin (DTMB) 5415.

The present study conducted CFD simulations under various roughness conditions. The roughness function determined by Demirel et al. (2017a) was embedded into the wall-functions of the CFD model to represent the surface scenario proposed by Schultz (2007). The simulations were performed with a range of speeds. Finally, the effects of biofouling on ship resistance components and flow characteristics around the hulls were investigated.

2   Methodology

2.1   Approach

Fig.1 illustrates the methodology employed in the current study. The Simcenter STAR-CCM+ (ver. 15.06) was utilised for the CFD simulations on a full-scale naval ship (DTMB 5415). The fouling conditions described by Schultz (2007) were applied to the simulations using the modified wall-function approach, incorporating the roughness function model proposed by Demirel et al. (2017a). Through these full-scale CFD simulations, the impact of different hull conditions was investigated regarding the increase in resistance and powering, as well as the speed reductions.
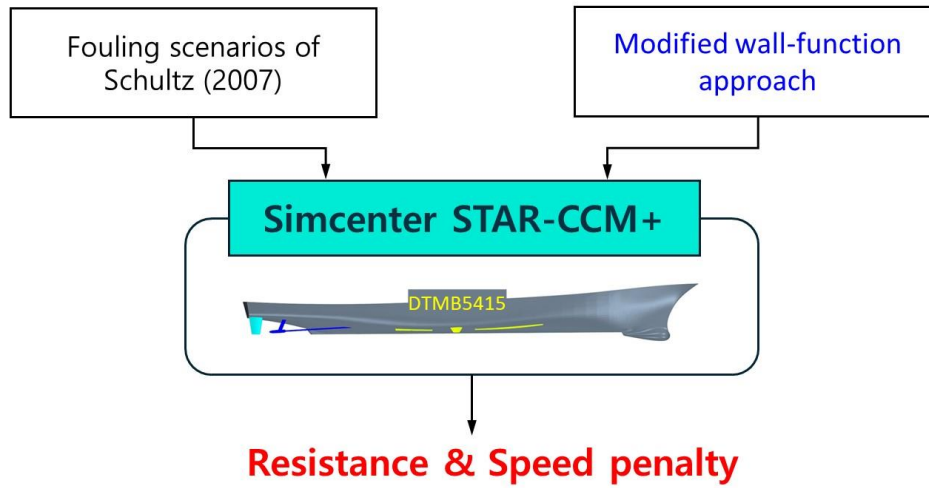
< Fig. 1 Diagram illustrating the flow of research >

2.2   Numerical modelling

2.2.1   Governing equation

The proposed CFD model was developed based on the Reynolds-averaged Navier-stokes (RANS) method using a commercial CFD software package, STAR-CCM+. As in the following two equations, the averaged continuity and momentum equations for incompressible flows may be given in tensor notation and Cartesian coordinates (Ferziger and Peric, 2002).

$$\frac{\partial(\rho u_i)}{\partial x_i} = 0, \qquad \cdots (1)$$

$$\rho \frac{\partial(u_i)}{\partial t} + \rho u_j \frac{\partial u_i}{\partial x_j} = -\frac{\partial P}{\partial x_i} + \frac{\partial}{\partial x_j}\left(2\mu S_{ij} - \rho \overline{u_i' u_j'}\right), \qquad \cdots (2)$$

$$S_{ij} = \frac{1}{2}\left(\frac{\partial u_i}{\partial x_j} + \frac{\partial u_j}{\partial x_i}\right) \qquad \cdots (3)$$

$$\rho\tau_{ij} = -\rho\overline{u_i'u_j'} \qquad \cdots(4)$$

Where the ρ is density, u is the averaged velocity vector, P is the averaged pressure, μ is the dynamic viscosity, $-\rho\overline{u_i'u_j'}$ is known as the Reynolds-stress tensor, S_{ij} is a strain-rate tensor and τ_{ij} is the specific Reynolds stress tensor.

The computational domains were discretised and solved using a finite volume method in the CFD solver. The second-order upwind convection scheme and a first-order temporal discretisation were employed for the momentum equations. The entire solution procedure is based on the semi-implicit method for the Pressure-Linked Equations (SIMPLE) type algorithm, which is composed of the continuity equation and the momentum equation and obtains the predicted velocity field that satisfies the continuity equation through pressure correction. The Shear Stress Transport (SST) k-ω was utilised to consider the effects of turbulence. For the simulation's free surface, the Volume of Fluid (VOF) method was used with High-Resolution Interface Capturing (HRIC).

2.2.2 Modified wall-function approach

This study utilised surface scenarios suggested by Schultz (2007) in Table 1, including Smooth, Typical anti fouling (AF) coating, Heavy slime, and Small calcareous fouling conditions. Within this context, k_s denotes the equivalent sand-grain roughness height, which represents the k_s of the sand-grain surface that has the same effect as the corresponding surface and is not a value measured on the surface. The modelling of these representative hull conditions was achieved using the roughness function proposed by Demirel et al. (2017a), as in equation (5).

$$\Delta U^+ = \begin{cases} 0 & \rightarrow & k^+ < 3 \\ \frac{1}{\kappa}\ln(0.26k^+)^{\sin\left[\frac{\pi}{2}\frac{\log(k^+/3)}{\log(5)}\right]} & \rightarrow & 3 \leq k^+ < 15 \\ \frac{1}{\kappa}\ln(0.26k^+) & \rightarrow & 15 \leq k^+ \end{cases} \qquad \cdots(5)$$

As shown in Fig. 2, Equation (5) agrees with observations in the entire regime of k^+ values.
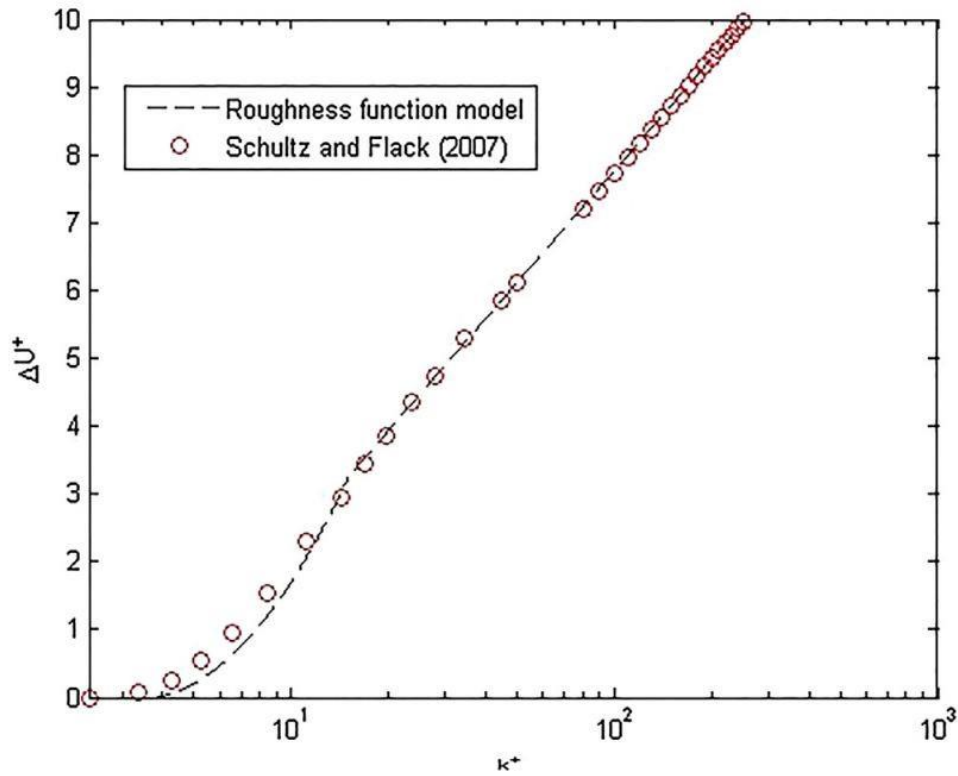
< Fig. 2 The proposed CFD roughness function model together with the roughness functions Demirel et al. (2017a) >

Table 1

A range of representative coating and fouling conditions Schultz (2007).

| Description of condition	NSTM rating	k_s (μm)	Rt_{50} (μm)
Hydraulically smooth surface	0	0	0
Typical as applied AF coating	0	30	150
Deteriorated coating or light slime	10-20	100	300
Heavy slime	30	300	600
Small calcareous fouling or weed	40-60	1000	1000
Medium calcareous fouling	70-80	3000	3000
Heavy calcareous fouling	90-100	10000	10000

2.3   *Geometry and boundary conditions*

This study utilised both model and full-scale DTMB 5415. The model scale DTMB 5415 was employed to validate against experimental data in its bare hull condition. Furthermore, the roughness effect was investigated using the fully appended full-scale DTMB 5415. Fig. 3 illustrates the hull geometry of the vessel, (a) is the hull in a bare hull condition without appendages, and (b) is the ship in a fully appended condition with rudder, strut, and bilge keel attached. Table. 2 represents the principal particulars.

Table. 3 shows the simulation cases used in this study. Both model and full-scale conducted free-surface

simulations have the free surface and hence consider the wave-making

(a)

(b)
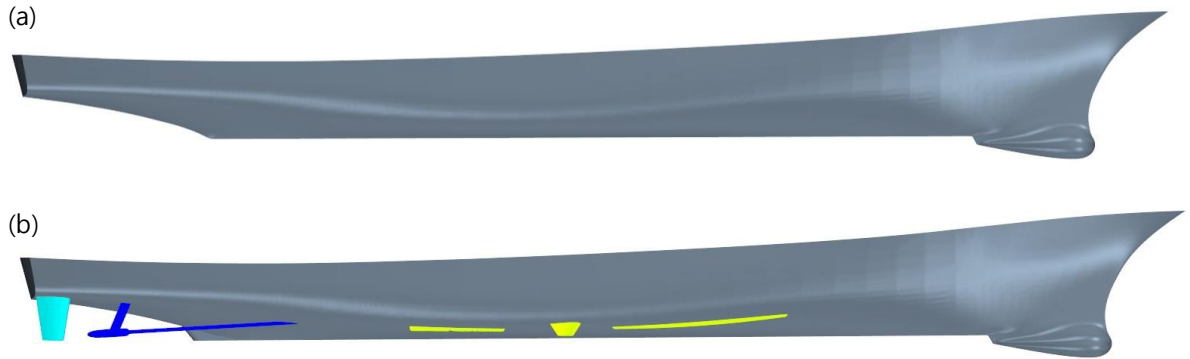
< Fig. 3 Geometry of the benchmark ship hulls of a navy surface combatant, DTMB 5415

(a) Bare hull, (b) Fully appended >

Table 2

Principal particulars and conditions of the DTMB 5415 simulations, adapted from Olivieri et al (2001).

Main particulars	Full-scale	Model-scale
Scale factor, λ	1	24.824
Length between the perpendiculars, L_{pp} (m)	142.0	5.720
Beam at the waterline, B_{wl} (m)	18.9	0.76
Design draught, T (m)	6.16	0.248
Wetted surface area without a rudder, S (m^2)	2949.5	4.786
Displacement, ∇ (m^3)	8636.0	0.549
Block coefficient, C_B	0.506	0.506

Table 3

Simulation cases

	Double-body	Free-surface	
	Full-scale	Full-scale	Model-scale
Scale factor, λ	1	1	24.824
Speed range, $V(m/s)$	7.48-15.30	7.48-15.30	1.501-3.071
F_n range	0.20-0.41	0.20-0.41	0.20-0.41
Re_L range	1.06×10^9-2.18×10^9	1.06×10^9-2.18×10^9	8.55×10^6-1.75×10^7
Surface condition	Smooth, Anti-fouling coating, Heavy slime, Small calcareous fouling		

6

(a) Double-body simulation   (a) Free-surface simulation
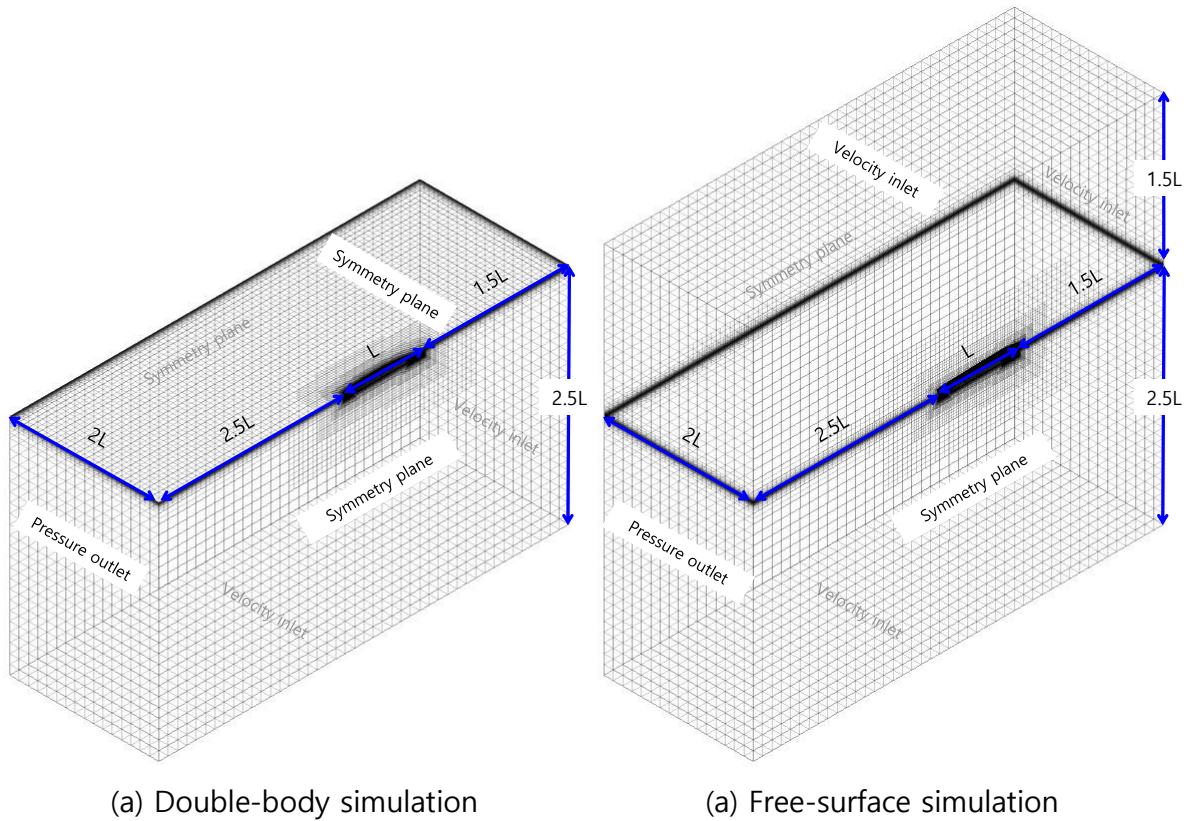
< Fig. 4 Computation domain and boundary condition of DTMB 5415 simulation >

Fig. 4 illustrates the computational domain and boundary condition of the double-body and free-surface simulations. Computational domain is a block with a length of 5L, a width of 2L and a height of 4L. The velocity inlet boundary condition was imposed at the computational domain's upstream (positive x-direction), top, and bottom walls. The side boundaries (the two opposite faces at the y-direction of the domain) were set as symmetry conditions, and the downstream (negative x-direction) was modelled as a pressure outlet condition. In the double-body simulations, the Z=0 plane is replaced with a symmetry plane, eliminating the free surface. It's important to note that all simulations were conducted under fixed conditions, meaning no sinkage or trim motions were allowed.

2.4   Mesh generation

Mesh generation was carried out utilising the STAR-CCM+ built-in automatic meshing facilities. Trimmed cell meshes were employed to create high-quality, flow-aligned hexahedral cells. Moreover, local refinements were applied to enhance the mesh quality in critical regions, including the area surrounding the

hull and the Kelvin wake region.

In this study, target y^+ values were set to 80 for the model and 500 for the full scale. To achieve these y^+ values, the prism layer meshes were used for near-wall refinement, and the thickness of the first layer cell on the surface adjusted accordingly (Kim et al., 2023b; Song et al., 2024b). Fig. 5 shows the volume meshes of the domain.
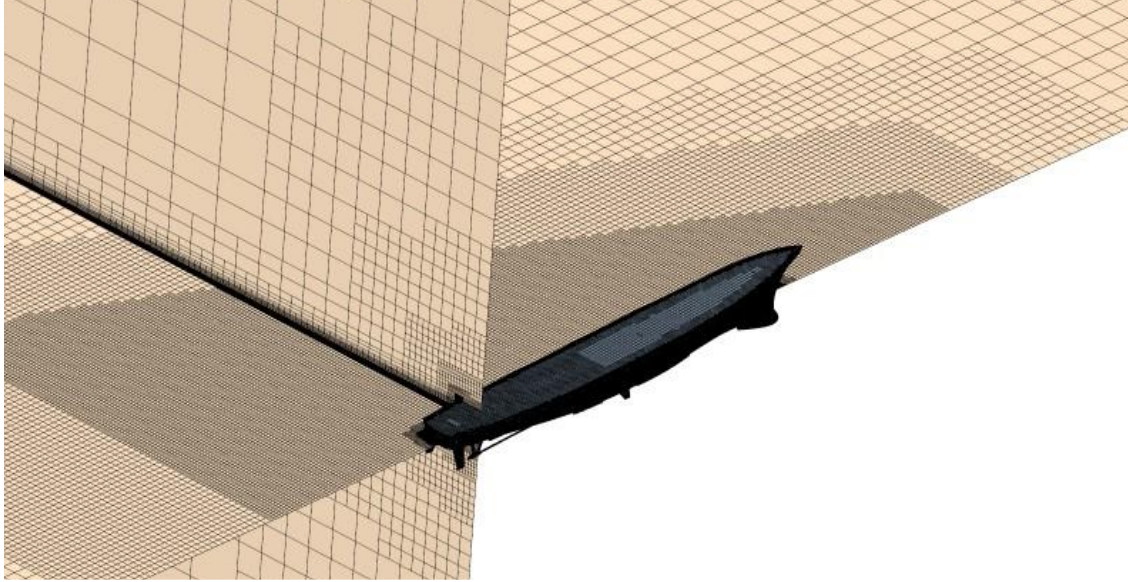
< Fig. 5 Mesh generation of the computation domain of DTMB 5415 >

3   Results

3.1   Verification and validation study

3.1.1 Verification study

A verification study was performed to ensure that the proper grid spacing, and time step were selected. Discretisation error estimation was performed using the Grid Convergence Index method (Celik et al, 2008). Tables. 4 and 5 show the results of the spatial and temporal convergence study of DTMB 5415 simulation. The spatial and temporal uncertainties were calculated based on the fine mesh and fine time step for each case. For accurate results, the fine mesh and fine time step were used in this study.

Table 4

Spatial and temporal convergence study of the Model-scale DTMB 5415 simulations. key variable: C_T

		Model-scale ($\lambda = 24.824$)	
Spatial convergence		No. Cells	C_T
	Coarse	622,365	6.513E-03
	Medium	1,206,746	6.584E-03
	Fine	2,486,593	6.597E-03
		U_{Grid}(Fine)	0.0392%

| Temporal convergence		Time step	C_T
	Coarse	0.02	6.527E-03
	Medium	0.01	6.590E-03
	Fine	0.005	6.597E-03
		$U_{\Delta t}$(Fine)	0.0146%

Table 5

Spatial and temporal convergence study of the Full-scale DTMB 5415 simulations. key variable: C_T

		Full-scale ($\lambda = 1$)	
Spatial convergence		No. Cells	C_T
	Coarse	862,973	5.786E-03
	Medium	1,682,139	5.548E-03
	Fine	3,256,735	5.503E-03
		U_{Grid}(Fine)	0.2515%
Temporal convergence		Time step	C_T
	Coarse	0.16	5.466E-03
	Medium	0.08	5.495E-03
	Fine	0.04	5.503E-03
		$U_{\Delta t}$(Fine)	0.2315%

3.1.2   Validation study

The validation study was conducted by comparing C_T value from the model-scale CFD simulation with the model test of Olivieri et al (2001) and CFD simulation results of Yaakob et al., (2015) and Firdhaus et al., (2021). The C_T value of DTMB 5415 simulations and model test of Olivieri et al (2001) were shown in Fig. 6. The simulation results, as depicted in Fig. 6, exhibited remarkable consistency with the experimental data.
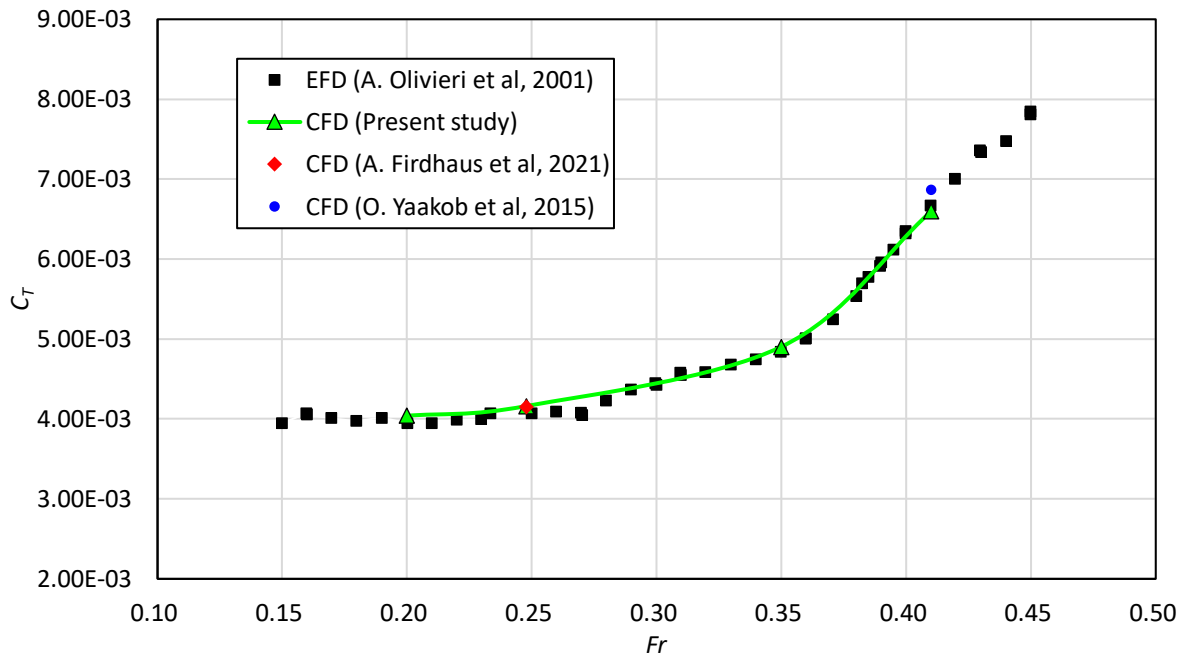
< Fig. 6 Comparison graph of CFD simulation and model experiment results >

3.2   Roughness effects on resistance component

3.2.1   Total resistance coefficient, C_T

To explore the impact of roughness on total resistance, C_T, simulations were conducted on the DTMB 5415. Fig. 7 illustrates the C_T value with and without the presence of hull fouling. It is evident from the Fig. 7 that hull fouling leads to a notable increase in C_T values. The figure demonstrates that accounting for the effect of hull roughness with typical anti fouling (AF) coating leads to the marked difference in the C_T value, with an increase of 4.7% at the operation speed (30 $knots$). Additionally, the percentage increase in the total resistance, i.e. %C_T, for the Heavy slime and Small calcareous fouling surface conditions at the operation speed is 15.4% and 23.7% respectively. The data indicate a more pronounced increase in the ship's total resistance at lower speeds compared to higher speeds. This trend can likely be attributed to the increasing dominance of frictional resistance as a component of total resistance at reduced speeds. Surface roughness is understood to predominantly affect frictional resistance rather than other types of resistance. The impact of surface roughness on frictional resistance will be examined in greater detail in the subsequent section.
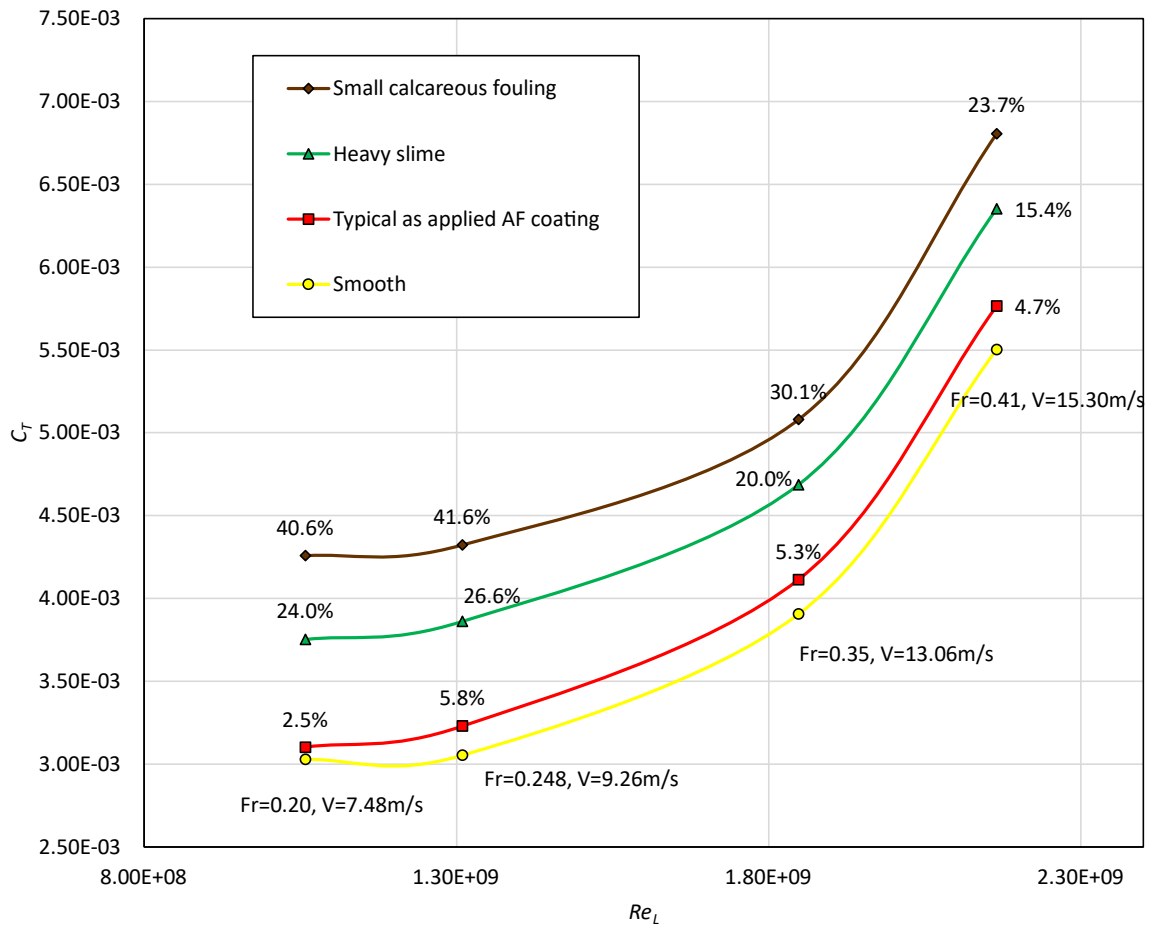
< Fig. 7 Total resistance coefficient, C_T, of DTMB 5415 with different hull conditions at full-scale >
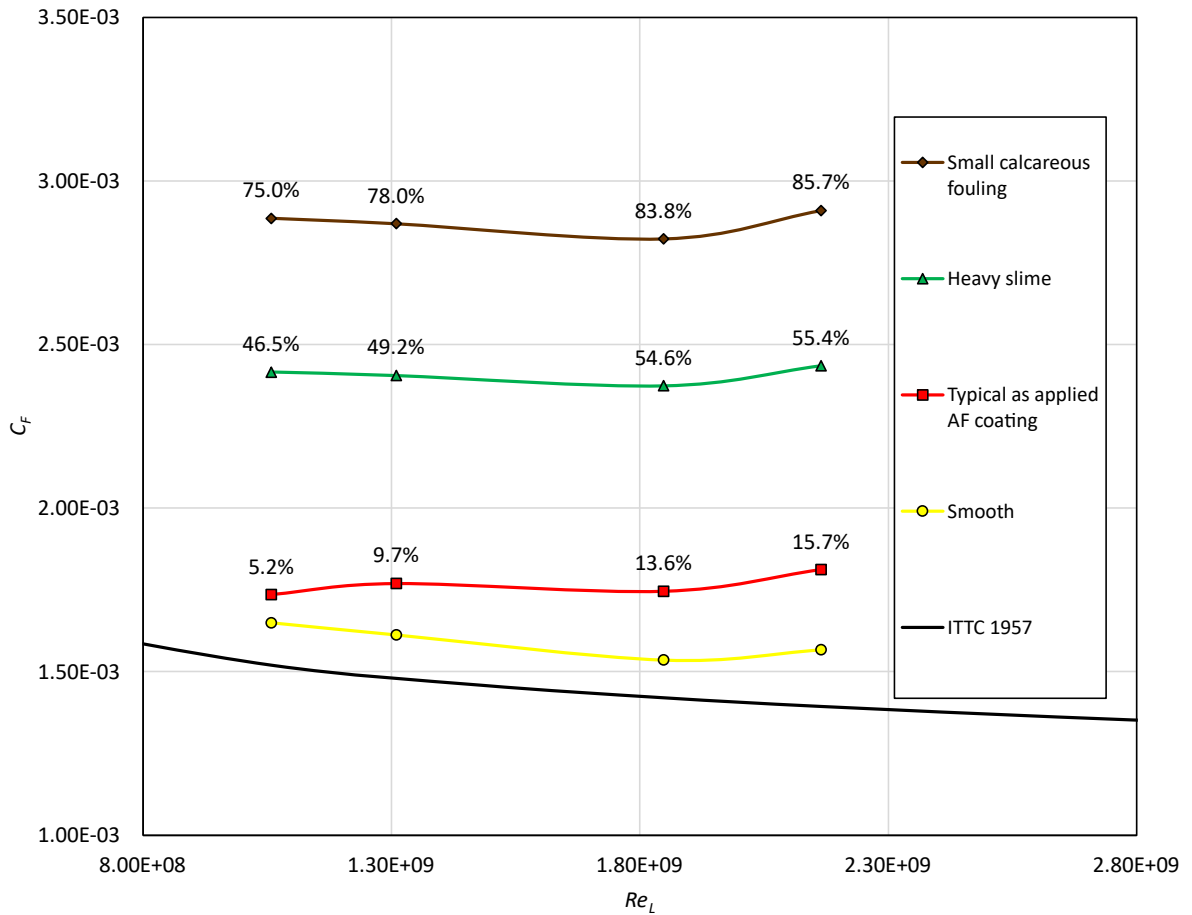
3.2.2 Frictional and Residual resistance coefficient, C_F and C_R

The total resistance coefficients, C_T, were disaggregated into the frictional resistance coefficients, C_F, and the residuary resistance coefficients, C_R, by dividing the total drag acting on the ship into the shear and pressure force components. Fig. 8 and 9 depict the frictional resistance, C_F and residuary resistance coefficients, C_R, obtained from the simulations. These values were directly derived from the full-scale DTMB 5415 simulation, considering shear (i.e. friction) and pressure (i.e. residuary) force components.

As shown in the Fig. 8, C_F values of the full-scale DTMB 5415 in smooth and fouled hull conditions (Typical anti fouling (AF) coating, Heavy slime, and Small calcareous fouling) experienced significant increases due to hull fouling. The predicted increase in the C_F values of DTMB 5415 at operation speed was predicted to be up to 85.7% under the most severe fouled conditions (Small calcareous fouling). Additionally, as depicted in Fig. 8, increases in frictional resistance diminish as speed increases and eventually transition into decreases at higher speeds. As shown in Fig. 10, the roughness function of Demirel et al. (2017a) used in this study reaches the fully rough regime when $k^+ > 15$. However, Fig. 8 indicates that this is not the case. This discrepancy arises because the resistance coefficient was calculated using the same wetted surface area (WSA) for each ship speed. Fig. 11 reveals that the WSA near bow, where the local skin friction is higher than other regions, increases at high speed. Therefore, although the fully rough regime was reached in all cases, it can be inferred that this result is due to the variation in WSA. Conversely, Fig. 9, shows that the increase in C_R values of DTMB 5415 exhibited relatively small increases and eventually transition into decreases at higher speeds. These trends, along with the increasing dominance of C_R and C_T for the DTMB 5415 case, can be correlated with the decreasing %ΔC_T values of DTMB 5415 as the speed

increases, as shown in Fig. 7. The results represented in Demirel et al., (2017a), the $\%\Delta C_F$ is from 10.9% to 76.9% for KCS. It is of note that the overall trends of C_F and C_R for DTMB 5415, tend to resemble those of a container ship (i.e. KCS) rather than a tanker (i.e. KVLCC2), as investigated by Demirel et al., (2017a) and Song et al. (2020c). In order to understand the rationale of the changing trends of the roughness effect on C_R, the residuary values were further decomposed into the wave-making resistance, C_W, and the viscous pressure resistance, C_{VP} and discussed in the following section.
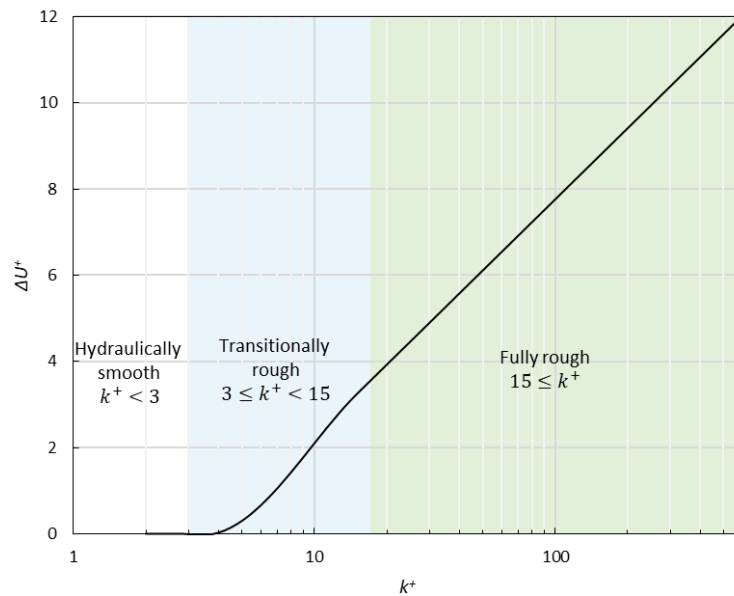

< Fig. 8 Frictional resistance coefficient, C_F, of DTMB 5415 with different hull conditions at full-scale >
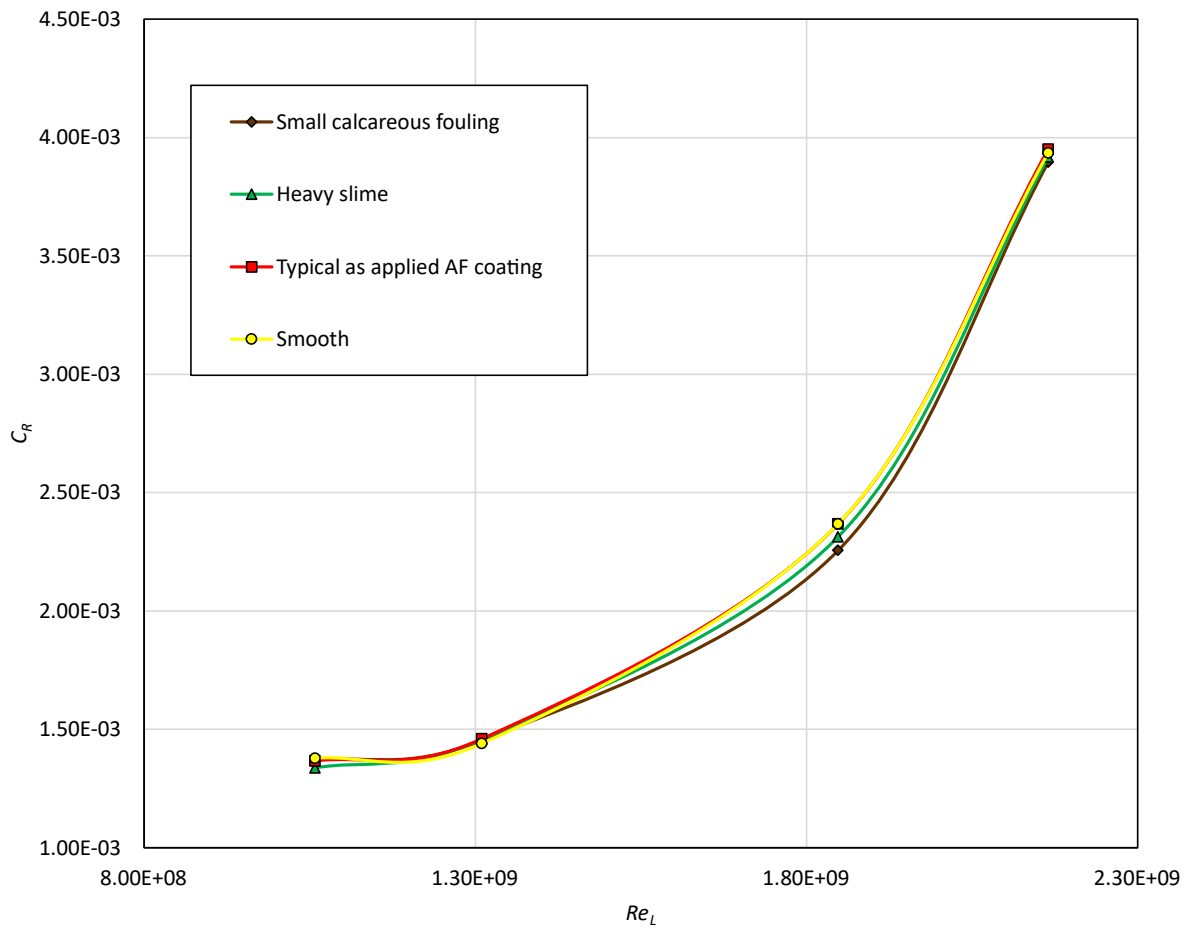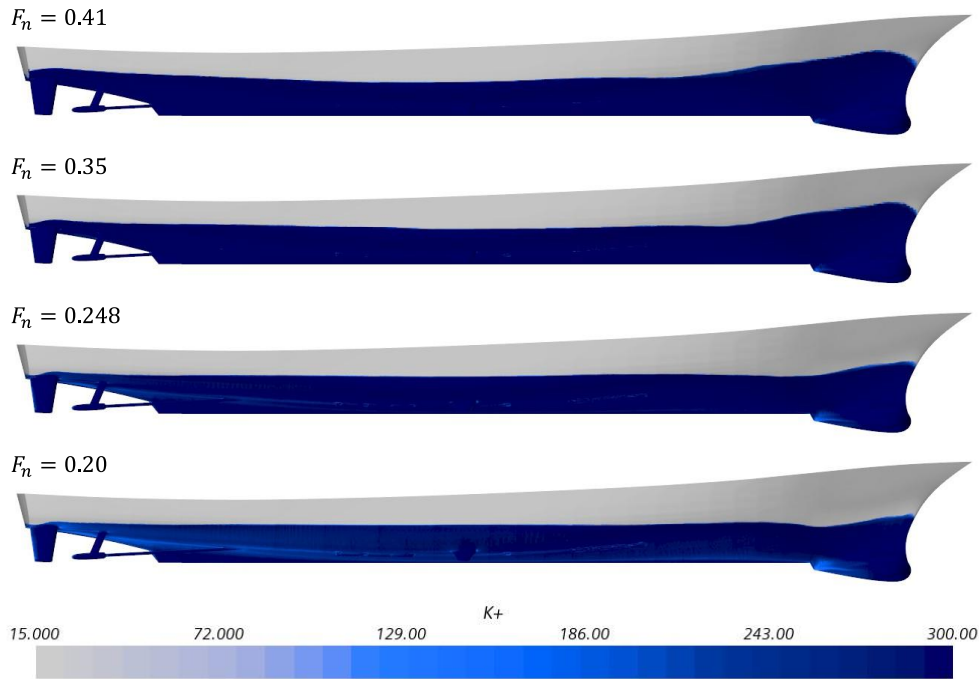
< Fig. 9 Residuary resistance coefficient, C_R, of DTMB 5415 with different hull conditions at full-scale >

< Fig. 10 Roughness function model of Demirel et al., 2017a >

$F_n = 0.41$

$F_n = 0.35$

$F_n = 0.248$

$F_n = 0.20$

$K+$

| 15.000 | 72.000 | 129.00 | 186.00 | 243.00 | 300.00 |

< Fig. 11 k^+ on the hulls of DTMB 5415 with small calcareous fouling condition >
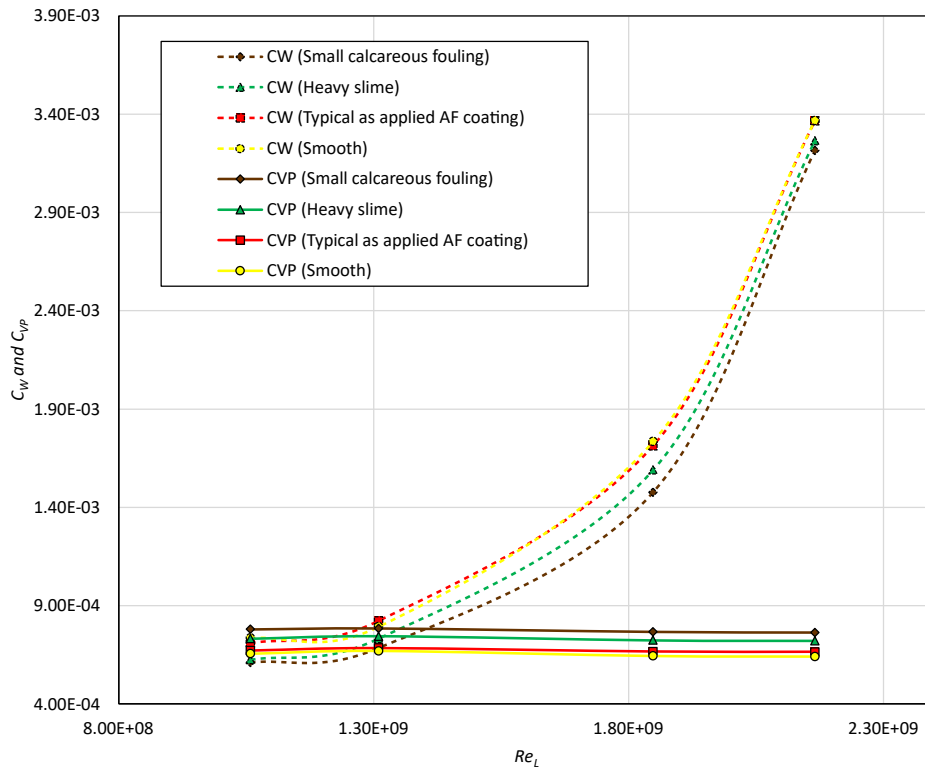
3.2.3   Wave-making and Viscous pressure resistance coefficient, C_W and C_{VP}

The residual resistance coefficient, C_R , can decomposed into wave-making resistance coefficient, C_W and viscous pressure resistance coefficient, C_{VP} . For the calculation of C_W and C_{VP} , the double-body simulations were performed. In the double-body simulation, the free surface is replaced with the double-body flow, representing the flow with a flat-water surface (Larsson and Raven, 2010). As a result, the free-surface effect is neglected so that total resistance, C_T , is equal to viscous resistance, C_V .

Fig. 12 illustrates the C_W and C_{VP} values for the full-scale DTMB 5415 under smooth and fouled conditions (AF coating, heavy slime, and small calcareous fouling). For C_{VP} , the DTMB 5415 shows percentage increases due to hull fouling, with %ΔC_{VP} values of 3.59%, 12.4%, and 19.0% for AF coating, heavy slime, and small calcareous fouling surface conditions, respectively, at the operational speed. For the DTMB 5415, C_W values significantly contribute to C_R and increase sharply with speed, eventually becoming dominant over C_{VP} . The overall trend is similar to KCS, but there are differences in increase/decrease rate. These differences can be attributed to various factors, (i.e. block coefficient, appendages, higher F_n). However, the increase in the dominance of C_W remains the same. Consequently, for the fouled DTMB 5415, the decreases in C_W counteract the increases in C_{VP} , eventually leading to a decrease in C_R at higher speeds.

< Fig. 12 Wave-making and Viscous pressure resistance coefficient, C_W and C_{VP}, of DTMB 5415 with different hull conditions at full-scale >

3.3   Speed penalty

For merchant ships, increased fuel consumption due to increased ship resistance is a major concern. However, in the case of warships, not only the increase in fuel consumption but also the speed reduction is an important factor to consider. For this purpose, the speed penalty at the operation speed was analysed, and in the calculation, the speed penalty was calculated based on the typical anti fouling (AF) coating conditions, not the smooth condition, to represent the ship speed reduction due to surface contamination during operation. Fig. 13 illustrates the increase in the P_E of the DTMB 5415 due to a biofouling. The increased in P_E because of biofouling can be expressed by

$$\%\Delta P_E = \frac{C_{T,rough} - C_{T,AF\ coating}}{C_{T,rough}} \times 100 \qquad \cdots (6)$$

Similar to that used by Tezdogan et al., (2015) and Demirel et al., (2017b).

To estimate the speed penalty due to the biofouling, an effective power curve is generated for each speed, and the reduced speed is determined for the constant P_E value of the AF coating. This is similar to the method used by Farkas et al., (2020a).

As can be seen in Fig. 13, the effective power continuously increased with increasing fouling rate. The results presented in Fig. 13 indicate that the increase in the P_E of DTMB 5415 due to Heavy slime and Small calcareous fouling at operation speed was predicted to be 10.4% and 16.6% respectively. Fig. 14 shows the decrease in speed due to increased resistance compared to the typical anti-fouling (AF) coating, there was a decrease in ship speed of 4.33% for heavy slime and 6.67% for Small calcareous fouling. This can act as a

major flaw in the warship's speed performance.
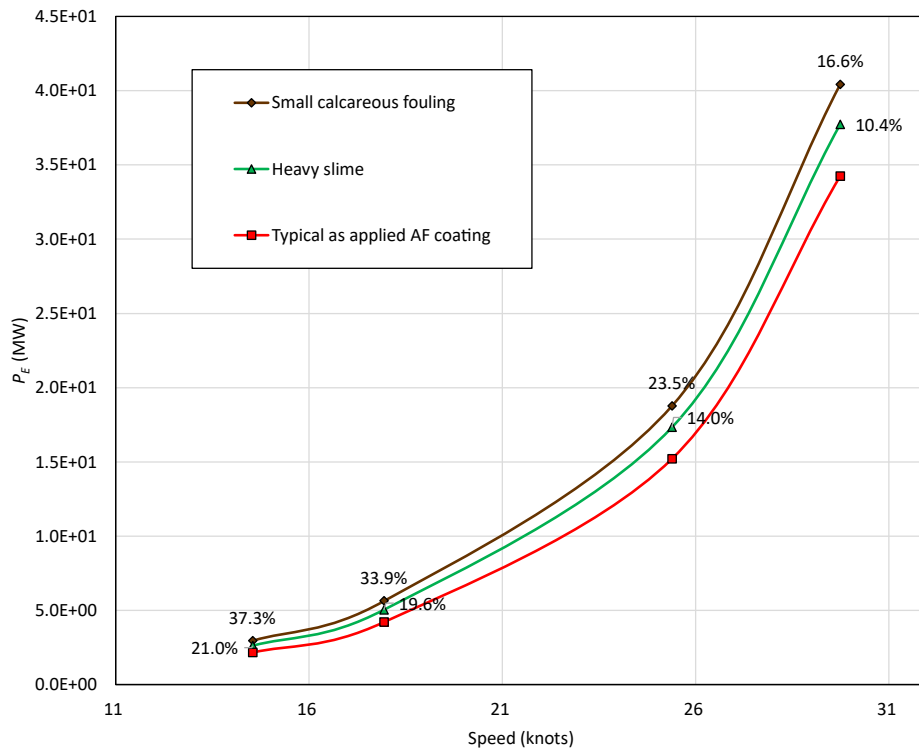
< Fig. 13 Estimation of the percentage increase in the effective power due to different surface conditions >
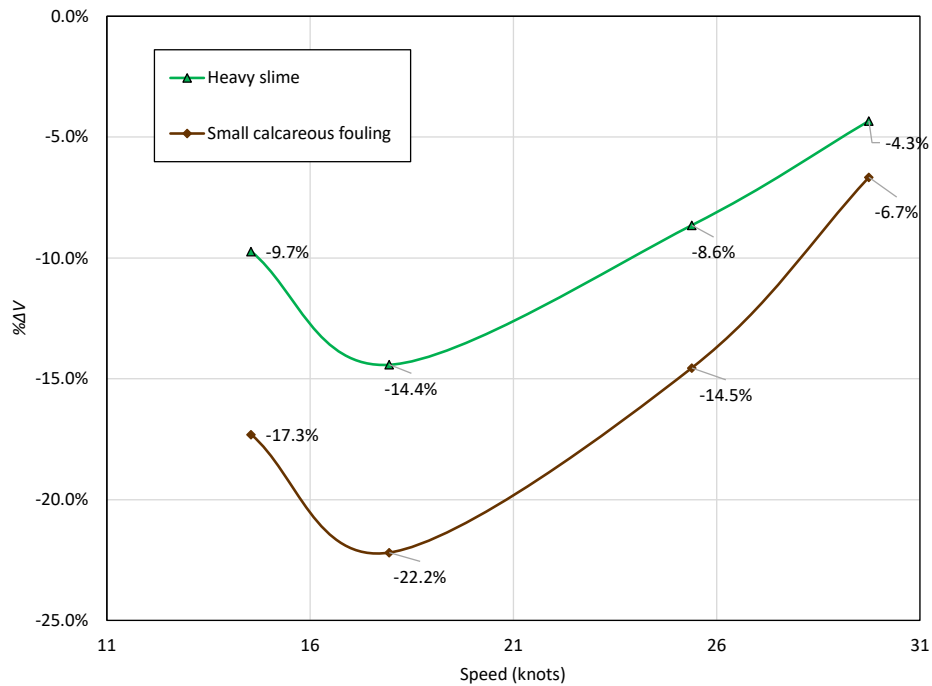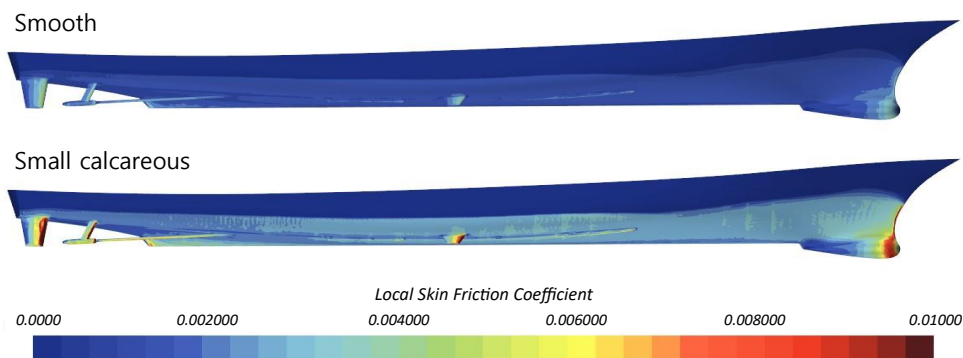

< Fig. 14 Speed penalty of DTMB 5415 (baseline: AF coating condition) >

3.4   Roughness effects on the hydrodynamic characteristics

3.4.1   Turbulent kinetic energy

Fig. 15 displays the contours of turbulent kinetic energy for DTMB 5415 under smooth and small calcareous fouling conditions. It is evident from Fig. 15 that turbulent kinetic energy rises with increased surface roughness, attributed to the presence of biofouling attachment. This increase in turbulence subsequently results in an elevation of local skin friction coefficient, as illustrated in Fig. 16 (Farkas et al., 2020a).
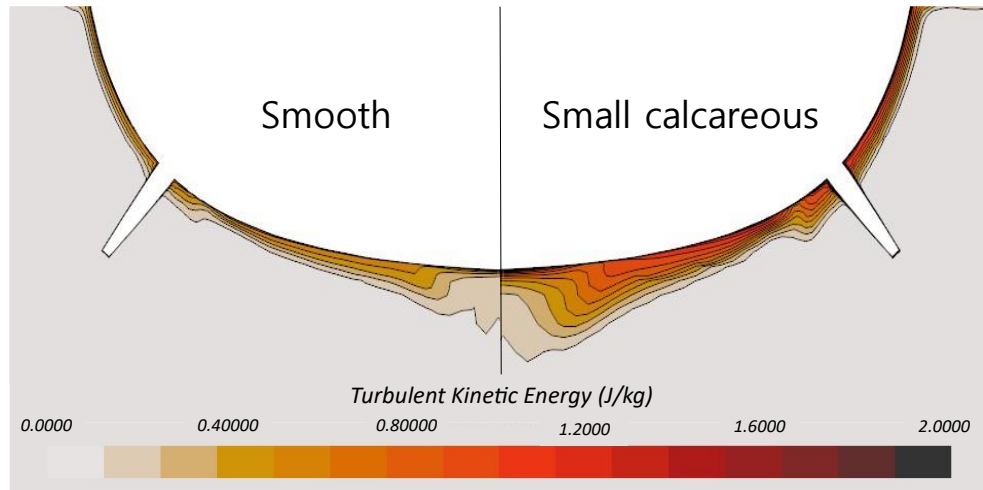
< Fig. 15 Turbulent kinetic energy of the DTMB 5415 for smooth and Small calcareous fouling
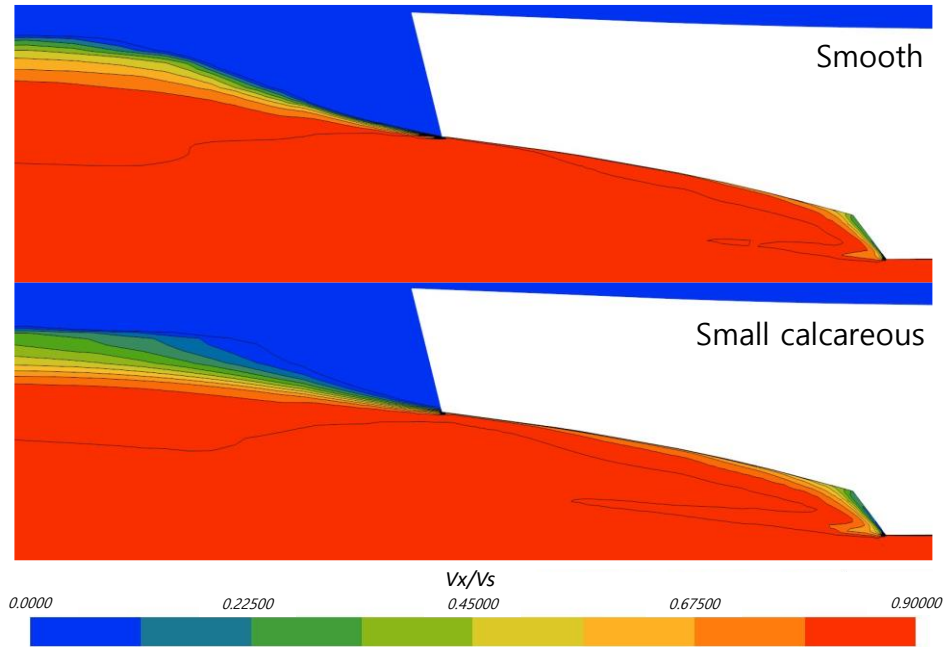
$(Fn = 0.41, 30 knots)$ >

< Fig. 16 Distribution of Local skin friction coefficient, C_f for smooth and Small calcareous fouling conditions
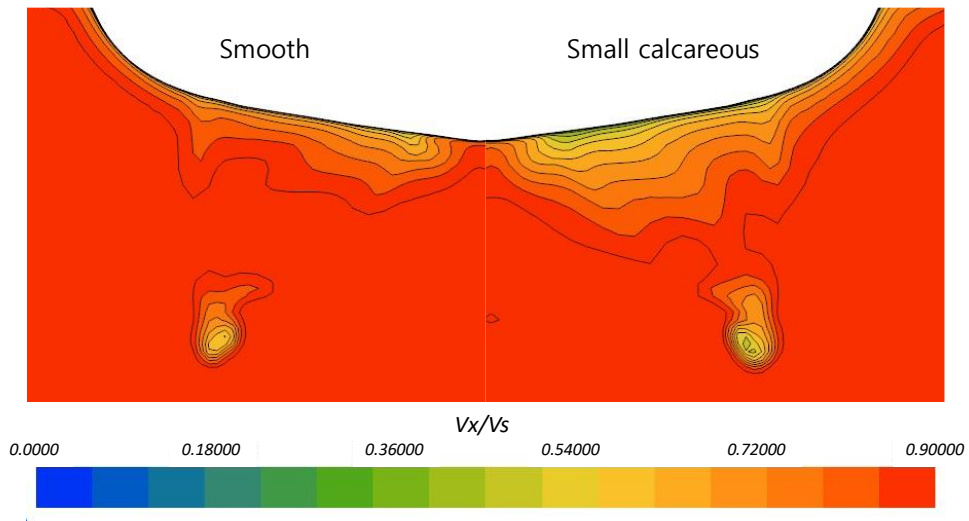$(Fn = 0.41, 30 knots)$ >

3.4.2   Velocity field

Fig. 17 presents the axial velocity contours around the stern of the DTMB 5415 under smooth surface conditions and the most severe fouling conditions (Small calcareous fouling) at the operational speed (30 knots). The mean axial velocity was normalised by dividing the local velocity by the ship's advance speed (V_x/V_{ship}), and the contours were captured on the $y = 0$ plane. As depicted in the figure, the roughness effect induces significant alterations in the velocity field around the hulls. Surface roughness causes a

deceleration of the flow velocity around the ship's stern, consequently expanding the wake field. This phenomenon is further highlighted in Fig. 18, which provides a comparison of axial velocity behind the hull in the propeller plane ($x = 0.9346L_{PP}$). This observation is consistent with the findings of recent studies (Farkas et al., 2020a; Song et al., 2019a).

< Fig. 17 Axial velocity (V_x/V_{ship}) around the stern in full-scale DTMB 5415 ($Fn = 0.41, 30knots$) >

< Fig. 18 Axial velocity (V_x/V_{ship}) at propeller plane in full-scale DTMB 5415 ($Fn = 0.41, 30knots$) >

3.4.3   Boundary layer thickness

Another notable feature of the fouling effect, as depicted in Fig. 19, is the augmentation in the boundary layer thickness, particularly noticeable on the hull bottom and the aft end region. Fig. 19 illustrates that the wake contours are influenced by surface roughness. In the rough case (small calcareous fouling), the wake

velocities are reduced, leading to an enlargement of the wake region due to surface roughness (Song et al., 2020c; Farkas et al., 2020b). The decelerated flow surrounding the hull bears implications for the ship's propulsion efficiency, as it influences the wake fraction encountered at the propeller section.
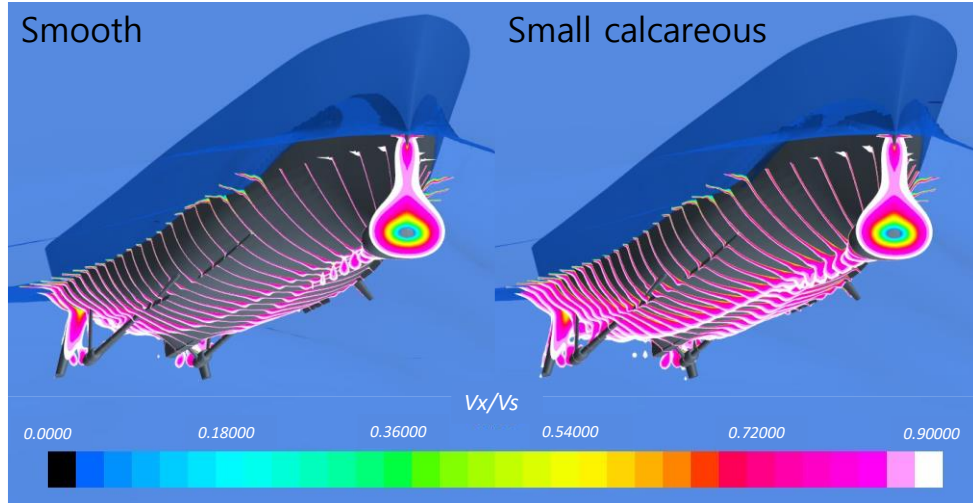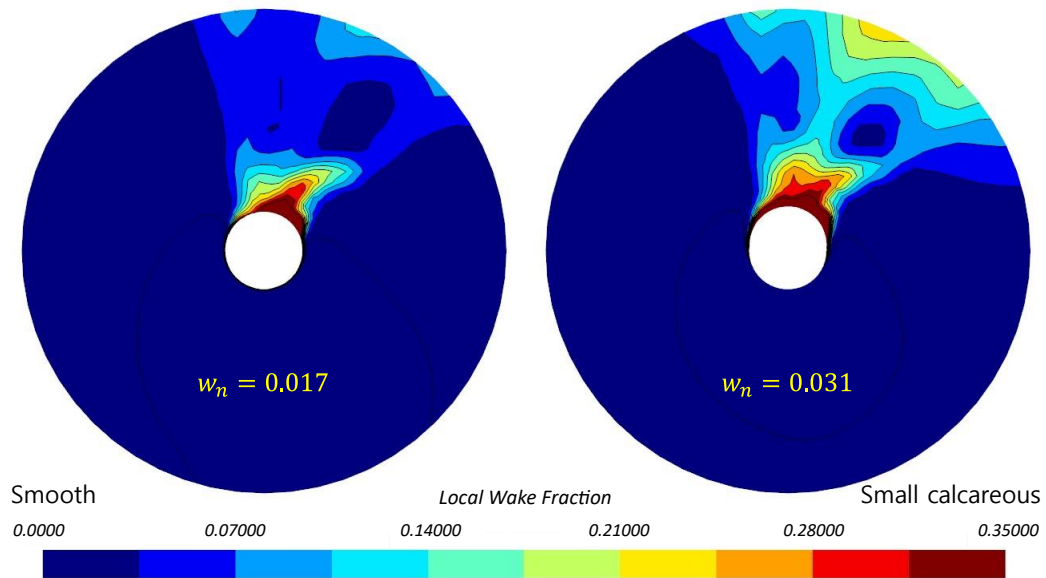

$<$ Fig. 19 Boundary layer representation around the hull (V_x/V_{ship}=0.9) ($Fn = 0.41, 30 knots$) $>$

3.4.4 Nominal wake

Fig. 20 represented the mean wake fraction, w_n, of the DTMB 5415 with the smooth and rough cases. The wake fraction is defined as follows.

$$w_n = 1 - V_x/V_{ship} \qquad \cdots (7)$$

The mean nominal wake fraction, w_n, was calculated by integrating the local wake fraction, w'_x, over the propeller disk region. In Fig 20, the inner circle represents the hub diameter while the outer circle corresponds to the propeller diameter. The increase in mean nominal wake fraction due to the biofouling can be up to 82% at operation speed. This observation aligns with the findings of recent studies (Farkas et al., 2019b; Song et al., 2019b). However, there is a variation in values, according to a previous study the increment of the nominal wake for KCS and KVLCC2 were 45% and 43% respectively (Song et al., 2020c). This is likely attributed to the difference in hull form (i.e., open skeg). Based on this finding, it might be anticipated that the rise in wake fraction could offset the adverse impact of hull fouling on the ship's resistance by enhancing hull efficiency. However, the slowed inflow at the propeller section also impacts propeller efficiency by changing the propeller advance coefficient. Therefore, to validate the impact of roughness on ship propulsion performance, further investigation is warranted through CFD simulations under self-propulsion conditions.

$w_n = 0.017$

$w_n = 0.031$

Smooth

Local Wake Fraction

Small calcareous

| 0.0000 | 0.07000 | 0.14000 | 0.21000 | 0.28000 | 0.35000 |

< Fig. 20 The mean wake fraction, w_n, at the propeller plane of DTMB 5415 ($Fn = 0.41, 30 knots$) >

4   Conclusion

With the aim of quantifying the resistance and speed penalty on a naval ship due to biofouling, we performed a URANS analysis with the benchmark ship hulls of a surface combatant, DTMB 5415.

To confirm the roughness effect in the resistance components of the ship and the decrease in ship speed according to the degree of roughness, four of the representative hull conditions presented by Schultz (2007) were used. To model the representative hull conditions, the roughness function model obtained by Demirel et al. (2017a) was adopted and embedded into the wall-function of the CFD model so that the surface boundary condition of the hull can represent the effect of biofouling.

Spatial and temporal convergence studies were conducted using the Grid Convergence Index (GCI) method to estimate the numerical uncertainties of the proposed CFD models and to determine appropriate grid spacings and time steps.

For the validation of the simulation, model-scale DTMB 5415 with bare hull condition simulation was conducted. The results obtained from the simulations showed good agreement with the experimental results of Olivieri et al. (2001) and CFD simulation results of Yaakob et al., (2015) and Firdhaus et al., (2021).

The ship resistance was decomposed into its components by using two different types of computational domains: double-body and free-surface. The results showed that the hull fouling causes significant increases in frictional resistance at varying speeds. For example, at operation speed, the increase in frictional resistance due to Small calcareous fouling condition was approximately 85.7% compared to smooth condition. Furthermore, the speed penalties were estimated to be 4.33% for heavy slime and 6.67% for small calcareous fouling, compared to typical anti-fouling coated conditions.

The effect of surface roughness on velocity distribution around the hull has been explored. It was observed that the surface roughness increases the boundary layer thickness and enlarges the wake region. Especially due to the increase in wake region in the stern of the ship, it was found that up to an 82% increase in nominal wake fraction can occur, which is likely to affect the propulsion performance of the ship.

The significant contribution of this study lies in broadening the scope of biofouling research to encompass

warships. However, the research has limitations that are not addressed in the current work. Specifically, in this simulation, the surfaces of the hull are assumed to be uniformly rough. In reality, the surfaces of actual ships are not uniform owing to the uneven accumulation of biofouling. This discrepancy can result in inaccurate predictions of resistance, suggesting a need for heterogeneous modelling of the hull surface, as indicated by Song et al. (2021) and Ravenna et al. (2022). Additionally, there is potential for extending the technology for modelling roughness effects to include ship manoeuvring characteristics, as highlighted by recent CFD studies by Kim et al. (2023a) and Song et al. (2024a). Consequently, future studies could focus the impact of hull roughness on the manoeuvring performance of warships.

5   *Acknowledgements*

6   *References*

A. Olivieri, F. P., A. Avanzini, F. Stern, R. Penna. (2001). Towing tank experiments of resistance, sinkage and trim, boundary layer, wake, and free surface flow around a naval combatant INSEAN 2340 model.

Brynolf, S., Baldi, F., & Johnson, H. (2016). Energy efficiency and fuel changes to reduce environmental impacts. Shipping and the Environment: Improving environmental performance in marine transportation, 295-339.

Celik, I. B., Ghia, U., Roache, P.J., Freitas, C.J., Coleman, H., Raad, P.E. (2008). Procedure for Estimation and Reporting of Uncertainty Due to Discretization in CFD Applications. Journal of Fluids Engineering, 130(7). https://doi.org/10.1115/1.2960953

Choi, H. J. (2015). Hull-form optimization of a container ship based on bell-shaped modification function. International Journal of Naval Architecture and Ocean Engineering, 7(3), 478-489. https://doi.org/10.1515/ijnaoe-2015-0034

Comas, J., Parra, D., Balasch, J. C., & Tort, L. (2021). Effects of Fouling Management and Net Coating Strategies on Reared Gilthead Sea Bream Juveniles. Animals (Basel), 11(3). https://doi.org/10.3390/ani11030734

Degiuli, N., Farkas, A., Martić, I., & Grlj, C. G. (2023). Optimization of Maintenance Schedule for Containerships Sailing in the Adriatic Sea. Journal of Marine Science and Engineering, 11(1). https://doi.org/10.3390/jmse11010201

Demirel, Y. K., Khorasanchi, M., Turan, O., Incecik, A., & Schultz, M. P. (2014). A CFD model for the frictional resistance prediction of antifouling coatings. Ocean Engineering, 89, 21-31. https://doi.org/https://doi.org/10.1016/j.oceaneng.2014.07.017

Demirel, Y. K., Song, S., Turan, O., & Incecik, A. (2019). Practical added resistance diagrams to predict fouling impact on ship performance. Ocean Engineering, 186. https://doi.org/10.1016/j.oceaneng.2019.106112

Demirel, Y. K., Turan, O., & Incecik, A. (2017a). Predicting the effect of biofouling on ship resistance using CFD. Applied Ocean Research, 62, 100-118. https://doi.org/10.1016/j.apor.2016.12.003

Demirel, Y. K., Uzun, D., Zhang, Y., Fang, H.-C., Day, A. H., & Turan, O. (2017b). Effect of barnacle fouling on ship resistance and powering. Biofouling, 33(10), 819-834. https://doi.org/10.1080/08927014.2017.1373279

Farkas, A., Degiuli, N., & Martić, I. (2019a). Impact of biofilm on the resistance characteristics and nominal wake. Proceedings of the Institution of Mechanical Engineers, Part M: Journal of Engineering for the Maritime Environment, 234(1), 59-75. https://doi.org/10.1177/1475090219862897

Farkas, A., Degiuli, N., Martić, I., & Dejhalla, R. (2019b). Numerical and experimental assessment of

nominal wake for a bulk carrier. Journal of Marine Science and Technology, 24(4), 1092-1104. https://doi.org/10.1007/s00773-018-0609-4

Farkas, A., Degiuli, N., & Martić, I. (2021). Assessment of the effect of biofilm on the ship hydrodynamic performance by performance prediction method. International Journal of Naval Architecture and Ocean Engineering, 13, 102-114. https://doi.org/10.1016/j.ijnaoe.2020.12.005

Farkas, A., Song, S., Degiuli, N., Martić, I., & Demirel, Y. K. (2020a). Impact of biofilm on the ship propulsion characteristics and the speed reduction. Ocean Engineering, 199. https://doi.org/10.1016/j.oceaneng.2020.107033

Farkas, A., Degiuli, N., Martić, I., & Dejhalla, R. (2020b). Impact of Hard Fouling on the Ship Performance of Different Ship Forms. Journal of Marine Science and Engineering, 8(10), 748. https://www.mdpi.com/2077-1312/8/10/748

Felayati, F. M., Cahyono, B., & Bakar, R. A. (2021a). Numerical investigation of dual-fuel engine improvements using split injection natural gas coupled with diesel injection timings at low load condition. International Journal on Engineering Applications, 9(1), 31-38.

Felayati, F. M., Cahyono, B., Bakar, R. A., & Birouk, M. (2021b). Performance and emissions of natural gas/diesel dual-fuel engine at low load conditions: Effect of natural gas split injection strategy. Fuel, 300, 121012.

Ferziger, J. H., Perić, M., & Street, R. L. (2002). Computational methods for fluid dynamics. springer.

Firdhaus, A., Suastika, I. K., Kiryanto, K., & Samuel, S. (2021). Benchmark Study of FINETM/Marine CFD Code for the Calculation of Ship Resistance [Benchmarking tests; CFD code; FINETM/Marine; Volume of fluid method; Ship resistance;]. 2021, 18(2), 8. https://doi.org/10.14710/kapal.v18i2.39727

Granville, P. S. (1958). The frictional resistance and turbulent boundary layer of rough surfaces. J. Ship Res. 2 (3), 52-74.

Granville, P. S. (1978). Similarity-law characterization methods for arbitrary hydrodynamic roughnesses. In: Granville, P.S. (Ed.). Final Report Naval Ship Research and Development Center, Bethesda, MD. Ship Performance Dept. David Tayler Naval Ship Research and Development Center, Bethesda, MD, p. 31.

Hakim, M. L., Firdaus, A., & Mursid, O. (2023). Investigating the comparison of ship resistance components between u and v-shaped hulls. Jurnal Teknologi, 85(3), 153-164. https://doi.org/https://doi.org/10.11113/jurnalteknologi.v85.19382

IMO. (2021). Resolution MEPC.331(76). AMENDMENTS TO THE INTERNATIONAL CONVENTION ON THE CONTROL OF HARMFUL ANTI-FOULING SYSTEMS ON SHIPS.

IMO. (2023). 2023 IMO Strategy on Reduction of GHG Emissions from Ships.

ITTC. (2021). Proceedings of the 29th Conference. Volume I,II. https://ittc.info/downloads/proceedings/29th-conference-2021-virtual/

Kim, D., Song, S., Turnock, S., & Tezdogan, T. (2023a). Nonlinear URANS model for path-following control problem towards autonomous marine navigation under wave conditions. Ocean Engineering, 270, 113681. https://doi.org/https://doi.org/10.1016/j.oceaneng.2023.113681

Daejeong Kim, Jeongbin Yim, Soonseok Song, Jun-Bum Park, Jongsung Kim, Yongung Yu, Khaled Elsherbiny, Tahsin Tezdogan, Path-following control problem for maritime autonomous surface ships (MASS) in adverse weather conditions at low speeds, Ocean Engineering, Volume 287, Part 2, 2023, 115860, ISSN 0029-8018, https://doi.org/10.1016/j.oceaneng.2023b.115860.

Larsson, L., Raven, H. C., & Paulling, J. R. (2010). Ship Resistance and Flow. Society of Naval Architects and Marine Engineers. https://books.google.co.kr/books?id=5zi8bwAACAAJ

Mohammad Danil, A., Frengki Mohamad, F., & Andi Haris, M. (2022). Flow Separation Evaluation on Tubercle Ship Propeller. CFD Letters, 14(4), 43-50. https://doi.org/10.37934/cfdl.14.4.4350

Monty, J. P., Dogan, E., Hanson, R., Scardino, A. J., Ganapathisubramani, B., & Hutchins, N. (2016). An assessment of the ship drag penalty arising from light calcareous tubeworm fouling. Biofouling, 32(4), 451–464. https://doi.org/10.1080/08927014.2016.1148140

Owen, D., Demirel, Y. K., Oguz, E., Tezdogan, T., & Incecik, A. (2018). Investigating the effect of biofouling on propeller characteristics using CFD. Ocean Engineering, 159, 505-516. https://doi.org/https://doi.org/10.1016/j.oceaneng.2018.01.087

Pullin, D., Hutchins, N., & Chung, D. (2017). Turbulent flow over a long flat plate with uniform roughness. Physical Review Fluids, 2(8), 082601.

Ravenna, R., Song, S., Shi, W., Sant, T., De Marco Muscat-Fenech, C., Tezdogan, T., & Demirel, Y. K. (2022). CFD analysis of the effect of heterogeneous hull roughness on ship resistance. Ocean Engineering, 258. https://doi.org/10.1016/j.oceaneng.2022.111733

Schultz, M. P. (2002). The Relationship between frictional resistance and roughness for surfaces smoothed by sanding. https://doi.org/10.1115/1.1459073兴

Schultz, M. P. (2004). Frictional Resistance of Antifouling Coating Systems. https://doi.org/10.1115/1.1845552兴

Schultz, M. P. (2007). Effects of coating roughness and biofouling on ship resistance and powering. Biofouling, 23(5-6), 331-341. https://doi.org/10.1080/08927010701461974

Schultz, M. P., Bendick, J. A., Holm, E. R., & Hertel, W. M. (2011). Economic impact of biofouling on a naval surface ship. Biofouling, 27(1), 87-98. https://doi.org/10.1080/08927014.2010.542809

Schultz, M. P., & Flack, K. A. (2007). The rough-wall turbulent boundary layer from the hydraulically smooth to the fully rough regime. Journal of Fluid Mechanics, 580, 381-405. https://doi.org/10.1017/S0022112007005502

Seok, W., Kim, G. H., Seo, J., & Rhee, S. H. (2019). Application of the Design of Experiments and Computational Fluid Dynamics to Bow Design Improvement. Journal of Marine Science and Engineering, 7(7). https://doi.org/10.3390/jmse7070226

Song, S., Demirel, Y. K., & Atlar, M. (2019a). An Investigation Into the Effect of Biofouling on Full-Scale Propeller Performance Using CFD Volume 2: CFD and FSI,

Song, S., Demirel, Y. K., & Atlar, M. (2019b). An investigation into the effect of biofouling on the ship hydrodynamic characteristics using CFD. Ocean Engineering, 175, 122-137. https://doi.org/https://doi.org/10.1016/j.oceaneng.2019.01.056

Song, S., Demirel, Y. K., & Atlar, M. (2020a). Penalty of hull and propeller fouling on ship self-propulsion performance. Applied Ocean Research, 94. https://doi.org/10.1016/j.apor.2019.102006

Song, S., Demirel, Y. K., & Atlar, M. (2020b). Propeller performance penalty of biofouling: Computational fluid dynamics prediction. Journal of Offshore Mechanics and Arctic Engineering, 142(6), 061901.

Song, S., Demirel, Y. K., De Marco Muscat-Fenech, C., Tezdogan, T., & Atlar, M. (2020c). Fouling effect on the resistance of different ship types. Ocean Engineering, 216. https://doi.org/10.1016/j.oceaneng.2020.107736

Song, S., Demirel, Y. K., De Marco Muscat-Fenech, C., Sant, T., Villa, D., Tezdogan, T., & Incecik, A. (2021). Investigating the Effect of Heterogeneous Hull Roughness on Ship Resistance Using CFD. Journal of Marine Science and Engineering, 9(2). https://doi.org/10.3390/jmse9020202

Song, S., Kim, D., Demirel, Y. K., & Yang, J. (2023). An advanced prediction method of ship resistance

with heterogeneous hull roughness. Ocean Engineering, 279, 114602. https://doi.org/https://doi.org/10.1016/j.oceaneng.2023.114602

Song, S., Kim, D., & Dai, S. (2024a). CFD investigation into the effect of GM variations on ship manoeuvring characteristics. Ocean Engineering, 291, 116472. https://doi.org/https://doi.org/10.1016/j.oceaneng.2023.116472

Soonseok Song, Woo-Seok Choi, Myeong-Jin Eom, Man Hwan Kim, Byoung Guk Kim, Townsin's formula vs CFD: Evaluating hull roughness effect in ship resistance, Ocean Engineering, Volume 303, 2024b, 117754, ISSN 0029-8018, https://doi.org/10.1016/j.oceaneng.2024.117754.

Taskar, B., & Andersen, P. (2020). Benefit of speed reduction for ships in different weather conditions. Transportation Research Part D: Transport and Environment, 85. https://doi.org/10.1016/j.trd.2020.102337

Tahsin Tezdogan, Yigit Kemal Demirel, Paula Kellett, Mahdi Khorasanchi, Atilla Incecik, Osman Turan, Full-scale unsteady RANS CFD simulations of ship behaviour and performance in head seas due to slow steaming, Ocean Engineering, Volume 97, 2015, Pages 186-206, ISSN 0029-8018,https://doi.org/10.1016/j.oceaneng.2015.01.011.

Townsin, R. L. (2003). The Ship Hull Fouling Penalty. Biofouling, 19(sup1), 9-15. https://doi.org/10.1080/0892701031000088535

Tran, T. G., Nguyen, H. V., & Huynh, Q. V. (2023). A method for optimizing the hull form of fishing vessels. Journal of Ship Research, 67(01), 72-91. https://doi.org/https://doi.org/10.5957/JOSR.05210017

Trimulyono, A., Hakim, M. L., Ardhan, C., Ahmad, S. T. P., Tuswan, T., & Santosa, A. W. B. (2023). Analysis of the double steps position effect on planing hull performances. Brodogradnja, 74(4), 41-72. https://doi.org/10.21278/brod74403

Tuswan, T., Sari, D. P., Muttaqie, T., Prabowo, A. R., Soetardjo, M., Murwantono, T. T. P., Utina, R., & Yuniati, Y. (2023). Representative application of LNG-fuelled ships: a critical overview on potential ghg emission reductions and economic benefits. Brodogradnja, 74(1), 63-83. https://doi.org/10.21278/brod74104

Yaakob, O., M. Ahmed, Y., Rashid, M. F. A., & Elbatran, A. H. (2015). Determining Ship Resistance Using Computational Fluid Dynamics (CFD). Journal of Transport System Engineering, 2(1), 20-25. https://jtse.utm.my/index.php/jtse/article/view/35

Zis, T. P. V., Psaraftis, H. N., & Ding, L. (2020). Ship weather routing: A taxonomy and survey. Ocean Engineering, 213. https://doi.org/10.1016/j.oceaneng.2020.107697